Neutrons on a surface of liquid helium

P. D. Grigoriev[*]
L. D. Landau Institute for Theoretical Physics, Chernogolovka, Moscow region, 142432, Russia

O. Zimmer[†]
Institut Laue-Langevin, 71 Avenue des Martyrs, CS 20156, F-38042 Grenoble Cedex 9, France

A. D. Grigoriev
Samara State University, Samara RU-443011, Russia

T. Ziman
Institut Laue-Langevin, 71 Avenue des Martyrs, CS 20156, F-38042 Grenoble Cedex 9, France
and LPMMC (UMR 5493), CNRS and Université Grenoble Alpes, BP 166, F-38042 Grenoble, France
(Received 1 October 2015; revised manuscript received 8 March 2016; published 22 August 2016)

We investigate the possibility of ultracold neutron (UCN) storage in quantum states defined by the combined potentials of the Earth's gravity and the neutron optical repulsion by a horizontal surface of liquid helium. We analyze the stability of the lowest quantum state, which is most susceptible to perturbations due to surface excitations, against scattering by helium atoms in the vapor and by excitations of the liquid, comprised of ripplons, phonons, and surfons. This is an unusual scattering problem since the kinetic energy of the neutron parallel to the surface may be much greater than the binding energies perpendicular. The total scattering time of these UCNs at 0.7 K is found to exceed 1 h, and rapidly increases with decreasing temperature. Such low scattering rates should enable high-precision measurements of the sequence of discrete energy levels, thus providing improved tests of short-range gravity. The system might also be useful for neutron β-decay experiments. We also sketch new experimental propositions for level population and trapping of ultracold neutrons above a flat horizontal mirror.

DOI: 10.1103/PhysRevC.94.025504

I. INTRODUCTION

The slow neutron plays an important role in low-energy particle physics as both an object in itself, in investigations of the properties of free neutrons, and as a tool to explore its interactions with known or hypothetical fields with high precision [1–3]. A particular class of experiments employs neutrons with energy lower than the neutron optical potential of typical materials, i.e., up to or order 300 neV. These so-called ultracold neutrons (UCNs) can be imprisoned for many hundreds of seconds in well-designed "neutron bottles". By virtue of the neutron magnetic moment of 60 neV/T, magnetic trapping is feasible, and also the gravitational interaction (100 neV per meter rise) can play a role in UCN storage and manipulation [4,5]. UCNs have found various applications, such as notably the longstanding search for a nonvanishing electric dipole moment of the neutron for detection of a new mechanism of CP violation [6–9], and measurements of the neutron lifetime as input for calculations of weak reaction rates in big-bang nucleosynthesis and stellar fusion [10,11], and for the determination of the weak axial-vector and vector coupling constants of the nucleon.

Discrete energy levels of UCNs in the Earth's gravitational field were proposed by Lushikov and Frank in 1978 [12], and demonstrated experimentally in the past decade [13–15]. A precise determination of the energies of these states, with characteristic sizes of several tens of micrometers, is an interesting tool for tests of various new scenarios of particle physics. Deviations from the Newtonian law of gravity at small distances can, for instance, be interpreted as a signal of large extra dimensions at the sub-millimeter scale [16,17] or as a hint for dark-energy "chameleon" fields [18,19]. A recent development, called gravity resonance spectroscopy (GRS), where transitions between levels are induced by vibrating the mirror, has paved a way towards sensitive tests of such scenarios [20]. An alternative, and competing, method will employ oscillating magnetic field gradients [21,22]. The GRS experiment described in Ref. [19] has already set stringent limits on chameleons (note, however, a strong atomic-physics competitor [23]). It has also constrained axion-like particles, improving the result of an analysis of the nonresonant gravity experiment described in Ref. [24]. A method not relying on spatial quantum states of the neutron employs spin precession of trapped UCNs close to a heavy mirror [25–27]. While this currently provides still higher sensitivity than previous GRS experiments, large gains may be expected from an adaptation of Ramsey's molecular beam technique of separated oscillatory fields to GRS [28]. Such a set-up has been proposed also for the search of a nonzero neutron charge [29].

All current experiments on gravitational quantum states of the neutron employ highly polished quartz mirrors. These are expensive, limited to sizes of several tens of centimeters, and they have to be horizontally levelled by some active means. In this respect, using a liquid surface as a mirror might initiate

[*]grigorev@itp.ac.ru
[†]zimmer@ill.fr

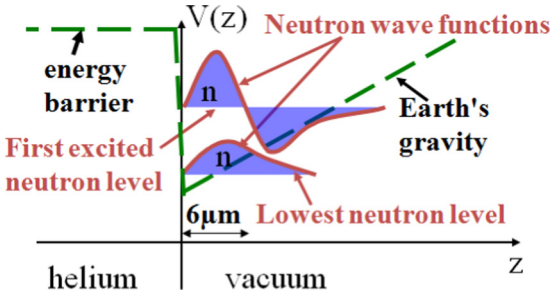

FIG. 1. Schematic representation of the vertical potential and the first two states of a neutron above a horizontal mirror of liquid helium.

a qualitatively new approach. The present article provides a theoretical investigation of the possibility to store UCNs in the lowest gravitational energy states on the liquid helium surface, by analysis of scattering by helium atoms in the gas phase and by various excitations in both the bulk and at the surface of the liquid helium. Obviously, a long storage time-constant is a necessary condition for conducting experiments using a mirror made of this quantum liquid. A separate section sketches some experimental concepts addressing issues arising in real studies employing those neutrons, notably population, trapping, and detection.

Properties of neutrons on the liquid helium surface are, in several respects, similar to those of electrons. The two-dimensional electron gas on a surface of dielectric media has been a wide subject of research for many decades (for reviews see, e.g., [30–32]). In contrast to the gravitational force in the neutron case, the electrons are attracted to the boundary by the electric image forces through which they become localized in the direction perpendicular to the surface. The surface of superfluid helium has no solid defects (like impurities, dislocations, etc.) and offers a unique opportunity to create an extremely pure 2D electron gas. The mobility of electrons in this gas usually exceeds by more than thousand times that of electrons in 2D quantum wells in heterostructures. The system thus simulates a solid-state 2D quantum well without disorder. Many fundamental properties of a 2D electron gas have been studied with the help of electrons on the surface of liquid helium. Various electronic quantum objects can be experimentally realized there, such as quantum dots [33], 1D electron wires [34], quantum rings [35], and so on. The electrons on the liquid helium surface may also serve for an experimental realization of a set of quantum bits with very long decoherence times [36]. If neutrons can be made to rest in surface states with sufficient densities we can hope for comparable studies using neutrons rather than electrons, investigations of excitations or structural decorations of the liquid surface detected by neutron scattering, and possible new states of quantum matter.

Without thermal excitations and above a flat helium surface such discrete neutron states can be easily described, as summarized in Sec. II and illustrated in Fig. 1. In Secs. III–V we consider the stability of a neutron in a bound surface state against various scattering processes. Note that we deal here with a rather unfamiliar scattering problem in that the kinetic energy of the neutron parallel to the surface may be many orders of magnitude greater than the binding energies in the perpendicular direction. We calculate the temperature-dependent scattering rates $w_{\rm vap}$ and $w_{\rm rip}$ due to ^{4}He atoms in the vapour above the surface and due to waves on the helium surface, called ripplons. Neutron scattering by other possible excitations, e.g., phonons and surfons, is also analyzed.

II. NEUTRONS ABOVE A FLAT HELIUM SURFACE

We consider a plane boundary between superfluid ^{4}He (situated at vertical coordinate $z < 0$) and its saturated vapor ($z > 0$). The interaction of a neutron with a ^{4}He atom with nuclear coordinate $\mathbf{R}_i$ can be expressed as a Fermi pseudopotential given by

$$V_i(\mathbf{r}) = U\delta^{(3)}(\mathbf{r}-\mathbf{R}_i) \equiv \frac{2\pi\hbar^2 a_{\rm He}}{m}\delta^{(3)}(\mathbf{r}-\mathbf{R}_i), \qquad (1)$$

where $\delta^{(3)}(\mathbf{r})$ is the 3D Dirac δ function. Substituting the bound coherent neutron scattering length $a_{\rm He} = 3.26\times10^{-13}$ cm of a ^{4}He atom and the neutron mass $m = 1.675\times10^{-24}$ g, one obtains the value $U = 1.36\times10^{-42}$ erg cm^3. Neutron propagation in the bulk (with particle density $n_{\rm He} \approx 21.8\,{\rm nm}^{-3}$ of ^{4}He atoms at $T < 2.18$ K) can be described by a constant neutron optical potential given by the spatially averaged pseudopotentials of many helium atoms in a volume Ω, i.e.,

$$V_0 = \Omega^{-1}\int_\Omega \sum_i V_i(\mathbf{r})d^3\mathbf{r} = Un_{\rm He} \approx 18.5\ {\rm neV}. \qquad (2)$$

Above the ^{4}He surface, neglecting interactions with the helium vapor discussed further below, the neutron is exposed to the gravity potential $V(z) = mgz$, where $g = 981$ cm/s^2. One can easily solve the one-dimensional Schrödinger equation for a neutron in this potential, sketched in Fig. 1. The corresponding Hamiltonian is

$$\hat{H}_0 = -\frac{\hbar^2\hat{\Delta}}{2m} + mgz + V_0\theta(-z), \qquad (3)$$

where $\hat{\Delta} = \nabla^2$ is the Laplace operator, and $\theta(x)$ is the step function [$\theta(x) = 1$ for $x > 0$ and $\theta(x) = 0$ for $x \leqslant 0$]. The x, y and z coordinates separate in this equation, and the neutron wave function is given by a product

$$\psi(\mathbf{r}) = \psi_\parallel(\mathbf{r}_{||})\,\psi_\perp(z), \qquad (4)$$

where $\mathbf{r}_{||} = (x,y)$ is the 2D coordinate vector along the surface, while $\mathbf{r} = (x,y,z)$ stands for the 3D coordinate vector. In the x-y plane, the neutron wave function is given by a normalized plane wave,

$$\psi_\parallel(\mathbf{r}_{||}) = S^{-1/2}\exp(i\mathbf{p}_{||}\mathbf{r}_{||}/\hbar), \qquad (5)$$

where S is the He surface area, and $\mathbf{p}_{||}$ is the 2D neutron momentum along the surface. At $z < 0$ one can neglect the weak gravitational potential in Eq. (3) as compared to the much stronger potential V_0. The z-dependent part of the neutron wave function in this region is then approximately given by

$$\psi_\perp(z) = \psi_\perp(0)\exp(\kappa z) \quad (z < 0,\ E_\perp < V_0), \qquad (6)$$

where $\kappa = ik_\perp = \sqrt{2m(V_0 - E_\perp)}/\hbar$, and $E_\perp$ is the neutron kinetic energy along the z axis. For $E_\perp \ll V_0$, $\kappa_0 \equiv \sqrt{2mV_0}/\hbar \approx$

2.4×10^5 cm^{-1}, i.e., the neutron penetration depth into the liquid helium is $\kappa_0^{-1} \approx 33$ nm. For $z > 0$, the neutron wave function is given by

$$\psi_\perp(z) = C\,\mathrm{Ai}[(z - E_\perp/mg)/z_0] \quad (z > 0), \tag{7}$$

where C is a normalization coefficient, $\mathrm{Ai}(x)$ is the Airy function, and $z_0 \equiv (\hbar^2/2m^2g)^{1/3} = 5.87\,\mu$m is a characteristic length scale of the neutron wave function in low energy states. For $z > E_\perp/mg$ the wave function given in Eq. (7) decreases exponentially. For $E_\perp < V_0$ the eigenvalues of the quantized energy spectrum are given by the boundary condition at $z = 0$, i.e.,

$$\frac{\psi_\perp'(0)}{\psi_\perp(0)} = \kappa = \frac{\sqrt{2m(V_0 - E_\perp)}}{\hbar} = \frac{\mathrm{Ai}'(-u)}{z_0\mathrm{Ai}(-u)}, \tag{8}$$

where $u \equiv E_\perp/mgz_0$ and primes denote derivatives. Equation (8) at finite V_0 can be solved only numerically. A characteristic scale of separations between lowest energy levels is given by $mgz_0 = (\hbar^2 mg^2/2)^{1/3} = 0.6$ peV. In the limit $V_0 \to \infty$ the energy levels are given by

$$E_n = mgz_0\alpha_{n+1}, \quad n = 0,1,\ldots, \tag{9}$$

where $-\alpha_{n+1}$ are the zeros of the Airy function. The lowest ones are given by $\alpha_1 = 2.338, \alpha_2 = 4.088$, $\alpha_3 = 5.521$, $\alpha_4 = 6.787$. For $n \gg 1$,

$$\alpha_n \approx (3\pi n/2)^{2/3} - (\pi^2/96n)^{1/3}. \tag{10}$$

At finite V_0, Eq. (8) gives the following values of $\alpha_{n+1}^{\mathrm{He}} = E_n/mgz_0$: $\alpha_1^{\mathrm{He}} = 2.332$, $\alpha_2^{\mathrm{He}} = 4.082$, $\alpha_3^{\mathrm{He}} = 5.515$, $\alpha_4^{\mathrm{He}} = 6.781$. They differ by less than 0.3% from α_n obtained at $V_0 \to \infty$. The neutron wave functions above the liquid He are also very close to those for $V_0 \to \infty$, except for a region near $z = 0$, where they acquire small finite values $\psi_{\perp n}(0) = C_n\,\mathrm{Ai}(-\alpha_{n+1}^{\mathrm{He}})$. The first three normalization coefficients are $C_0 \approx 59$ cm$^{-1/2}$, $C_1 \approx 51.3$ cm$^{-1/2}$, $C_2 \approx 47.8$ cm$^{-1/2}$, which gives $\psi_{\perp 0}(0) \approx 0.236$ cm$^{-1/2}$, $\psi_{\perp 1}(0) \approx -0.231$ cm$^{-1/2}$, $\psi_{\perp 2}(0) \approx 0.23$ cm$^{-1/2}$. These values enter the neutron scattering rate by ripplons and will be used below.

III. SCATTERING OF NEUTRONS IN SURFACE STATES BY HELIUM VAPOR

^{4}He vapor atoms can be considered as point-like impurities with interaction potential given by Eq. (1). The corresponding matrix element of the neutron scattering by He vapor atom is given by (see Appendix A for its standard derivation)

$$|T_{if}|^2 \approx U^2\,(2\pi\hbar)^3\delta^{(3)}(\Delta\mathbf{P}_{\mathrm{tot}})/V, \tag{11}$$

where the three-dimensional Dirac delta function $\delta^{(3)}(\Delta\mathbf{P}_{\mathrm{tot}})$ ensures the conservation of the total momentum $\mathbf{P}_{\mathrm{tot}}$. The helium vapor approximately obeys the Boltzmann distribution[1]

$$N_P = \exp\left(\frac{\mu - E_{\mathrm{He}}}{k_{\mathrm{B}}T}\right), \tag{12}$$

where $k_{\mathrm{B}} = 1.38 \times 10^{-16}$ erg/K is the Boltzmann constant, $\mu = -7.17$ K $\times\, k_{\mathrm{B}}$ is the chemical potential of liquid ^{4}He (evaporation energy of a ^{4}He atom) for $T \to 0$, and $E_{\mathrm{He}} = \mathbf{P}^2/2M$ is the kinetic energy of a ^{4}He atom with momentum $\mathbf{P}$ and atomic mass $M = 6.7 \times 10^{-24}$ g.

We take the initial neutron state on the lowest energy level along the z axis and with momentum $\mathbf{p}_{||} = \{p_x, p_y\}$ parallel to the helium surface, corresponding to the total neutron energy

$$K = p_{||}^2/2m + E_0. \tag{13}$$

In typical experiments with UCNs, $K \approx p_{||}^2/2m \sim 10^{-7}$ eV $\gg E_0 \sim 10^{-12}$ eV. The typical initial momentum $\mathbf{P}$ of a He atom is larger than the neutron momentum by more than an order of magnitude, because its average kinetic energy $\bar{E}_{\mathrm{He}} = (3/2)k_{\mathrm{B}}T \sim 10^{-4}$ eV is by about three orders of magnitude larger than the UCN energy K. Below [Eq. (17)] we will see that, as $p_{||} \to 0$, the neutron-He scattering rate w_{vap} remains finite, and we can neglect $p_{||}/P \ll 1$ in the calculation of this rate.

The scattering rate of a neutron with initial in-plane momentum $\mathbf{p}_{||}$ by a He atom with initial momentum $\mathbf{P}$ is given by the Fermi's golden rule [37]:

$$w_{\mathbf{P}} = \frac{2\pi}{\hbar}\int\frac{d^3\mathbf{P}'}{(2\pi\hbar)^3}\int\frac{Vd^3\mathbf{p}'}{(2\pi\hbar)^3}|T_{if}|^2\delta(\varepsilon - \varepsilon'). \tag{14}$$

Here $\varepsilon \approx P^2/2M$ and $\varepsilon' = P'^2/2M + (\mathbf{p} - \mathbf{p}')^2/2m$ are the initial and final total energies of He-atom and neutron. We now substitute Eq. (11) into Eq. (14). The integration over $\mathbf{p}'$ cancels $\delta^{(3)}(\Delta\mathbf{P}_{\mathrm{tot}})$ in Eq. (11), where $\Delta\mathbf{P}_{\mathrm{tot}} \approx \mathbf{P} - \mathbf{P}' - \mathbf{p}'$. After the integration over the angle ϕ between $\mathbf{P}$ and $\mathbf{P}'$ we obtain

$$w_{\mathbf{P}} = \int\frac{P'^2dP'}{2\pi\hbar^4}\frac{mU^2}{PP'} \times\theta\left[2PP' - \left|P^2\left(1 - \frac{m}{M}\right) + P'^2\left(1 + \frac{m}{M}\right)\right|\right]. \tag{15}$$

Since $M \approx 4m$, Eq. (15) simplifies to

$$w_{\mathbf{P}} \approx \int\frac{P'^2dP'}{2\pi\hbar^4}\frac{mU^2}{PP'}\theta[8PP' - 3P^2 - 5P'^2]. \tag{16}$$

The integrand is nonzero when $3/5 < P'/P < 1$, thus defining the range of integration in Eq. (16), i.e.,

$$w_{\mathbf{P}} = \int_{3P/5}^{P}\frac{P'dP'}{2\pi\hbar^4}\frac{mU^2}{P} = \frac{U^2Pm}{2\pi\hbar^4}\frac{8}{25}. \tag{17}$$

Finally, to obtain the total scattering rate as a function of temperature one has to integrate Eq. (17) over the initial He-atom momentum $\mathbf{P}$, weighted with the distribution function

[1]Since the chemical potential of liquid helium $|\mu| \gg k_{\mathrm{B}}T$, the Boltzmann distribution of He vapor almost coincides with the Bose-Einstein distribution.

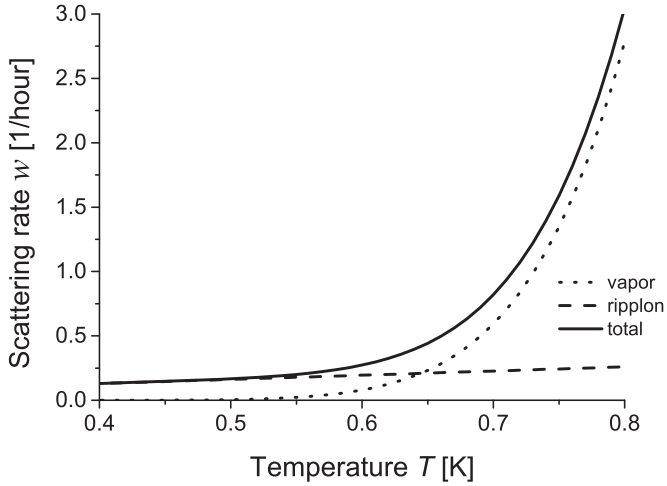

FIG. 2. The calculated total scattering rate (solid line) of UCNs on the liquid helium surface in inverse hours. The dotted and dashed lines give the contributions due to helium vapor and ripplons, respectively.

N_P of He vapor given by Eq. (12):

$$w_{\rm vap}(T) = \int \frac{d^3\mathbf{P} N_P}{(2\pi\hbar)^3} w_{\mathbf{P}} = \frac{(Mk_{\rm B}T)^2}{(\pi\hbar)^3} \frac{8mU^2}{50\hbar^4} e^{\mu/k_{\rm B}T}. \quad (18)$$

After substitution of Eq. (1) this gives the value of the neutron scattering rate by He vapor as function of temperature:

$$w_{\rm vap}(T) = 9.44\ {\rm s}^{-1} \times (T[{\rm K}])^2 \times \exp\left(\frac{-7.17}{T[{\rm K}]}\right). \quad (19)$$

Lowering the temperature this scattering rate decreases faster than exponentially, as illustrated in Figs. 2 and 3 at $T > 0.7$ K. Numerical values $w_{\rm vap}(1\ {\rm K}) \approx 0.007\ {\rm s}^{-1} = (138\ {\rm s})^{-1}$ and $w_{\rm vap}(T = 0.8\ {\rm K}) \approx 7.74 \times 10^{-4}\ {\rm s}^{-1} = (21.53\ {\rm min})^{-1}$ show, that the break-even with neutron decay is reached slightly above 0.8 K.

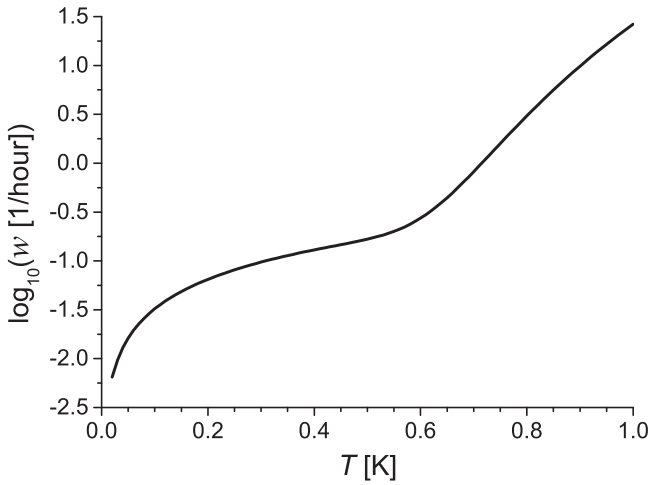

FIG. 3. The logarithm with base 10 of the calculated total scattering rate of UCNs on the liquid helium surface.

IV. SCATTERING FROM SURFACE WAVES

A. General information about ripplons

A quantum of a surface wave (ripplon) with momentum $\mathbf{q}$ induces a surface deformation along the z axis, given by

$$\xi(\mathbf{r}_\parallel, t) = \xi_{0q} \sin(\mathbf{q}\mathbf{r}_\parallel - \omega_q t). \quad (20)$$

The dispersion relation of surface waves is given by [30,38]

$$\omega_q^2 = \frac{\alpha}{\rho}(q^2 + \varkappa^2) q \tanh(qd), \quad (21)$$

where $\alpha \approx 0.354$ dyn/cm is the surface tension coefficient of superfluid ^{4}He, $\rho \approx 0.145$ g/cm^3 is its mass density, d is the depth of the helium bath above a horizontal bottom wall, and $\varkappa^2 = (g + f)\rho/\alpha$ with an additional force $f \propto d^{-4}$ due to the van der Waals attraction of helium to the bottom wall. The ripplon amplitude ξ_{0q} in Eq. (20), normalized to one ripplon per surface area S, is given by[2]

$$\xi_{0q} = \left(\frac{\hbar q \tanh(qd)}{2S\,\rho\omega_q}\right)^{1/2}. \quad (22)$$

For a helium bath (in fact already for a thick helium film), $\varkappa = \sqrt{g\rho/\alpha} \approx 20\ {\rm cm}^{-1}$. The thermal ripplons with energy $\hbar\omega_q \approx k_{\rm B} \times 0.5$ K have the wave number $q \approx 1.2\ {\rm nm}^{-1}$, for which holds $q \gg \varkappa$ and $qd \gg 1$. Then the dispersion relation of ripplons is just the dispersion of capillary waves:

$$\omega_q \approx \sqrt{\alpha/\rho} q^{3/2}, \quad (23)$$

and their amplitude

$$\xi_{0q} \approx \left(\frac{\hbar}{2S\sqrt{\rho\alpha q}}\right)^{1/2}. \quad (24)$$

At large wave vector $q \gtrsim 10\ {\rm nm}^{-1}$ the ripplon spectrum softens [40] as compared to Eq. (23), but we do not reach this limit because the thermal ripplons at temperature $T < 1$ K have smaller q.

B. Interaction Hamiltonian

To determine the influence of a periodic surface deformation on the neutron quantum state on the surface we have to separate two limits. The first, *adiabatic* limit occurs when the surface oscillates so slowly that the neutron wave function adjusts to the instantaneous surface profile. The interaction potential in this limit is found in Appendix B, see Eq. (B8), and can be rewritten as

$$\hat{H}_{\rm int} = \xi(\mathbf{r}_\parallel, t)\left\{\left[\frac{(\hat{p}_\parallel + \hat{p}_q)^2 - \hat{p}_\parallel^2}{2m} - \hbar\omega_q\right]\frac{\partial}{\partial z} + mg\right\}, \quad (25)$$

where $\hat{p}_\parallel = -i\hbar\nabla_\parallel$ and $\hat{p}_q = \hbar q$ are the momentum operators of the neutron and ripplon along the surface, respectively. This interaction term generalizes Eq. (7) of Ref. [28], because it

[2]Equation (22) can be obtained [30,39] by equating the energy of a classical surface wave with the wave number q and amplitude ξ_{0q} on the area S, given in §12, 25, 62 of Ref. [38], to the energy $\hbar\omega_q$ of one ripplon.

does not exclude coordinate-dependent surface perturbations. The expression in the square brackets in Eq. (25) is just the transfer of the total (neutron+ripplon) kinetic energy to the final neutron kinetic energy along the z axis.

The opposite, antiadiabatic or *diabatic* limit occurs when the surface oscillates much faster than the characteristic frequency of the out-of-plane neutron motion, so that the neutron wave function does not adjust to the instantaneous surface profile. In this limit a surface wave affects the neutrons by creating an additional time- and coordinate-dependent periodic potential

$$V_r(\mathbf{r}_\parallel,z) = \begin{cases} V_0 \text{ at } 0 < z < \xi(\mathbf{r}_\parallel,t) & \text{for } \xi(\mathbf{r}_\parallel,t) > 0 \\ -V_0 \text{ at } \xi(\mathbf{r}_\parallel,t) < z < 0 & \text{for } \xi(\mathbf{r}_\parallel,t) < 0 \end{cases}. \tag{26}$$

The ripplon amplitude, given by Eqs. (22) or (24), for any reasonable value of S is much less than the atomic scale and, even more, than the typical scale of the neutron wave function, given by $\kappa_0^{-1} \approx 33$ nm at $z < 0$. Therefore, the potential in Eq. (26) can be approximated by

$$V_r(\mathbf{r}) \equiv V_r(\mathbf{r}_\parallel,z) \approx V_0 \xi(\mathbf{r}_\parallel,t)\delta(z). \tag{27}$$

C. Crossover between adiabatic and diabatic limits and matrix elements

The adiabatic-diabatic crossover, corresponding to a change of the ripplon-neutron interaction Hamiltonian from Eq. (26) to Eq. (25), must take place when the ripplon frequency ω_q and the wave vector $\mathbf{q}$ decrease. However, the estimate of the crossover frequency ω_{qc} and the description of the system in the crossover regime is not a trivial problem. A similar problem occurs in other condensed-matter systems and requires a special theoretical study (see, e.g., Refs. [41–45]).

One may, naively, define the crossover as the region where the ripplon frequency becomes comparable to the quasiclassical bouncing frequency of a neutron in the ground level in z direction, i.e., when the ratio $\hbar\omega_q/E_0 \sim 1$, where E_0 given by Eq. (9). This corresponds to the ripplon frequency

$$\omega_{qc} \sim E_0/\hbar = 915 \text{ s}^{-1}, \tag{28}$$

and to the wave number $q_c \approx (\omega_{qc}^2\rho/\alpha)^{1/3} = 70 \text{ cm}^{-1} > \varkappa$. However, such an estimate of the adiabatic-diabatic crossover has an important drawback: it does not depend on the value V_0 of the neutron potential of the helium mirror. Generally, we expect that for $V_0 \to 0$ and for nonzero q and ω_q one can always apply Eq. (26), and for $V_0 \to \infty$ one can always apply Eq. (25), which contradicts Eq. (28). The classical definition of the adiabatic-diabatic crossover, given by Eqs. (C5) and (C6) in Appendix C, has the same drawback.

A rigorous analysis of the adiabatic-diabatic crossover should be based on the solution of the Schrödinger equation for a neutron in the time-dependent potential given by Eqs. (B1) and (B2). One may approximately determine the criterion of adiabatic-diabatic crossover from the variational principle to minimize the neutron energy. This approach would be strict for a time-independent potential, while for a potential periodic in time it is approximate. The lowest-level out-of-plane neutron wave function adjusts to minimize the neutron energy. In the adiabatic limit the energy loss/gain is the kinetic and gravitational energy from Eq. (25), while in the diabatic limit it is the potential energy from Eq. (26). The first-order correction $\Delta_{(1)}E_n$ to the neutron energy is given by the diagonal matrix elements of these two interaction potentials. If these diagonal matrix elements are nonzero, their comparison gives the crossover frequency. If these matrix elements vanish in the first order in ξ, one needs to calculate and compare the second-order corrections, which also include the nondiagonal matrix elements.

Since $\int_{-\infty}^{\infty} dz \psi_{\perp 0}^*(z)\partial\psi_{\perp 0}(z)/\partial z = 0$, and also $\int \xi(\mathbf{r}_\parallel,t)\, d^2\mathbf{r}_\parallel = 0$, the first-order (in ξ) diagonal matrix element of the adiabatic Hamiltonian in Eq. (25) vanishes. So does the diagonal matrix element of the diabatic Hamiltonian in Eq. (26) in the first order in ξ, if $\mathbf{p}_{||} \neq \hbar\mathbf{q}$. Hence, to calculate the crossover frequency one needs to calculate the second-order energy corrections, which do not vanish. These corrections are determined, in particular (but not only), by the matrix elements of the neutron-ripplon interaction potentials in Eqs. (25) and (26). Therefore, for an estimate of the position (ripplon frequency) of the adiabatic-diabatic crossover the comparison of the matrix elements, given below, is more accurate than just the comparison of ripplon frequency with $E_0/\hbar$.

A rough estimate of the crossover between the diabatic and adiabatic limits is given by the ripplon frequency when two interaction Hamiltonians, given by Eqs. (26) and (25), become of the same order of magnitude. More precisely, we compare their matrix elements for the neutron transitions between lowest energy levels of their motion in z direction. Thus defined, the adiabatic-diabatic crossover depends on V_0 and meets other general requirements, such as the adiabatic limit for $\omega_q, q \to 0$. The matrix element T_{if} of the diabatic interaction potential in Eq. (27) for the transitions between two neutron states with initial wave function $\psi_\perp(z)$ and final wave function $\psi'_\perp(z)$, written explicitly in Eqs. (4)–(7), is given by

$$T_{if} = \int \frac{d^3\mathbf{r}}{S} \psi_\perp(z)\psi'^*_\perp(z) \exp\left(i\mathbf{r}_{||}\frac{\mathbf{p}_{||} - \mathbf{p}'_\parallel}{\hbar}\right) V_0\xi(\mathbf{r}_\parallel)\delta(z).$$

The integral over z cancels $\delta(z)$, while after substituting Eq. (20) the integration over $\mathbf{r}_{||}$ gives $(2\pi\hbar)^2\delta^{(2)}(\Delta\mathbf{p}_{\text{tot}||})$, where $\Delta\mathbf{p}_{\text{tot}||} = \hbar\mathbf{q} + \mathbf{p}_{||} - \mathbf{p}'_\parallel$ is the change of the total in-plane momentum of the ripplon+neutron system. As a result we obtain

$$T_{if} = V_{||}V_{0,n}\,. \tag{29}$$

The factor

$$V_{||} = S^{-1}(2\pi\hbar)^2\delta^{(2)}(\Delta\mathbf{p}_{\text{tot}||}) \tag{30}$$

is due to the in-plane part $\psi_\parallel(\mathbf{r}_{||})$ of the neutron wave function, given by Eq. (5), and

$$V_{0,n} = V_0\xi_{0q}\psi^*_{\perp 0}(0)\psi_{\perp n}(0) \tag{31}$$

comes from its out-of-plane part $\psi_\perp(z)$. The squared modulus of the matrix element in Eq. (29) follows as

$$|T_{if}|^2 = \frac{(2\pi\hbar)^2\delta^{(2)}(\Delta\mathbf{p}_{\text{tot}||})}{S}\left|\psi_\perp(0)\psi'^*_\perp(0)V_0\xi_{0q}\right|^2, \tag{32}$$

where we again have used Eq. (A6).

The matrix elements of the adiabatic interaction potential in Eq. (25) for $\xi(\mathbf{r}_\parallel,t)$ given by Eq. (20) are

$$\hat{H}_{k,n} = V_{||}\xi_{0q}(E_k - E_n)Q_{k,n}, \tag{33}$$

where $V_{||}$ is again given by Eq. (30), and

$$Q_{k,n} = \int_0^\infty dz\psi^*_{\perp k}(z)\frac{d\psi^*_{\perp n}(z)}{dz}. \tag{34}$$

The first values of $Q_{k,n}$ are quoted in Table I of Ref. [28], e.g., $Q_{0,1} = 0.09742\ \mu\text{m}^{-1}$, $Q_{0,2} = -0.05355\ \mu\text{m}^{-1}$, $Q_{0,3} = 0.03831\ \mu\text{m}^{-1}$, $Q_{0,4} = -0.0304\ \mu\text{m}^{-1}$. Substituting these values we obtain for the first levels the ratio $V_{0,n}/\hat{H}_{0,n} \approx 1$ at

$$\omega_{qc} \approx 10^3\ \text{s}^{-1}. \tag{35}$$

By chance, the adiabatic-diabatic crossover condition, defined as $V_{0,n} \sim \hat{H}_{0,n}$, is close to the value quoted in Eq. (28).

Below, we consider the neutron-ripplon interaction in the diabatic limit, corresponding to the ripplon frequency $\omega_q > \omega_{qc}$ and the interaction potential given by Eq. (27), because it deals with much larger phase space of ripplons and because, as we will see later, the main contribution to the neutron-ripplon scattering rate comes from the ripplons with energy $\hbar\omega_q \sim V_0 \gg \hbar\omega_{qc}$, which corresponds to the far diabatic limit. Thus the final result is not sensitive to the value of the crossover frequency. Naturally our discussion of the crossover between adiabatic and diabatic limit is simplified and restricted to the lowest order. While this is an interesting general question, which clearly merits further discussion, we will not pursue the issue further here, as we shall only work in the diabatic limit. We remark that in discussions of the effects of driven oscillations of the interface of solid substrates, the opposite, adiabatic, limit is used as it is appropriate because of the large amplitudes and very low frequencies.

D. Absorption of ripplons

The scattering rate w_{rip} of a neutron with initial in-plane momentum $\mathbf{p}_{||}$ on ripplons is determined by two processes: the absorption and the emission of a ripplon with wave vector $\mathbf{q}$ and energy $\hbar\omega_q$,

$$w_{\text{rip}} = w_{\text{abs}} + w_{\text{em}}. \tag{36}$$

Since for typical ^{4}He temperatures k_BT is much larger than the initial neutron energy K, the populations of ripplon states within the relevant energy range are $N_q \gtrsim 1$ or even $N_q \gg 1$. The phase volume of an absorbed ripplon is much larger than that of an emitted ripplon, because the energy of the latter is limited to the initial kinetic energy of the neutron, $K \ll k_BT$. Hence, one could expect that the ripplon-neutron scattering rate is dominated by ripplon absorption, so that $w_{\text{rip}} \approx w_{\text{abs}}$. However, because of a low-energy divergence of w_{rip} (see below), the emission of low-energy ripplons with energies $\hbar\omega_{qc} < \hbar\omega_q \ll K$ may also be important, and we therefore consider both these processes.

The absorption scattering rate w_{abs} of a neutron with initial in-plane momentum $\mathbf{p}_{||}$ in the discrete vertical level with energy E_0 is given by the Fermi's golden rule,

$$w_{\text{abs}} = \frac{2\pi}{\hbar}\int\frac{N_qSd^2\mathbf{p}_q}{(2\pi\hbar)^2}\int\frac{Sd^2\mathbf{p}'_\parallel}{(2\pi\hbar)^2}\sum_n|T_{if}|^2\delta(\varepsilon-\varepsilon'), \tag{37}$$

where $\mathbf{p}_q \equiv \hbar\mathbf{q}$ is the ripplon momentum, and $\mathbf{p}'_\parallel = \mathbf{p}_\parallel + \mathbf{p}_q$ and n are the in-plane momentum and out-of-plane quantum number of the final neutron state, respectively:

$$N_q = [\exp(\hbar\omega_q/k_BT) - 1]^{-1} \tag{38}$$

is the Bose distribution function of ripplons with energy $\hbar\omega_q$ and with zero chemical potential. The matrix element $|T_{if}|$ is given by Eq. (32) and the initial total energy by

$$\varepsilon = \hbar\omega_q + \mathbf{p}^2_\parallel/2m + E_0. \tag{39}$$

The final energy $\varepsilon' = \mathbf{p}'^2_\parallel/2m + E_n$, after using the in-plane momentum conservation expressed by the δ function in Eq. (32), can be rewritten as

$$\varepsilon' = \frac{p^2_\parallel + p^2_q + 2p_qp_\parallel\cos\phi}{2m} + E_n, \tag{40}$$

where ϕ is the angle between $\mathbf{p}_\parallel$ and $\mathbf{p}_q$. The integration over the component $\mathbf{p}'_\parallel$ of the final neutron momentum parallel to the surface cancels the δ function in Eq. (32). After substitution of Eqs. (32), (39), and (40) to Eq. (37) we obtain

$$w_{\text{abs}} = \int\frac{N_qSp_qdp_qd\phi}{2\pi\hbar^3}\sum_n\left|\psi_{\perp0}(0)\psi^*_{\perp n}(0)V_0\xi_{0q}\right|^2 \times\delta\left(\hbar\omega_q - \Delta E_n - \frac{p^2_q + 2p_qp_\parallel\cos\phi}{2m}\right), \tag{41}$$

where $\Delta E_n = E_n - E_0 \approx E_n$ is the change of the out-of-plane neutron energy after the ripplon absorption. The integration over ϕ cancels the δ function in Eq. (41) and gives

$$w_{\text{abs}} = \int_0^\infty\frac{N_qSp_qdp_q}{\pi\hbar^3}\sum_n\frac{\left|\psi_{\perp0}(0)\psi^*_{\perp n}(0)V_0\xi_{0q}\right|^2}{\sqrt{a^2-(b-\Delta E_n)^2}}, \tag{42}$$

where $a \equiv p_\parallel p_q/m$ and $b \equiv \hbar\omega_q - p^2_q/2m$.[3] We estimate this integral in Appendix D. This calculation gives an upper bound of w_{abs} [see Eqs. (D11), (D17), and (D21)]:

$$w^{\text{up}}_{\text{abs}} \approx w^{\text{up}}_{>} + w^{\text{up}}_{<} + w^{\text{up}}_{\ll} \approx 7\times10^{-5}\times T[\text{K}]\ \text{s}^{-1}. \tag{43}$$

This corresponds to a mean neutron scattering time due to ripplon absorption of $\tau_{\text{rip}} > 4$ h even at $T = 1$ K.

E. Emission of ripplons

The rate of emission of a ripplon by a surface-state neutron with momentum $\mathbf{p}_\parallel$ is again given by Fermi's golden rule in Eq. (37), but now $\mathbf{p}' = \mathbf{p}_\parallel - \mathbf{p}_q$, the initial total energy is

[3]The integrand in Eq. (42) is real at $b - a \leqslant \Delta E_n \leqslant b + a$. The quantity $b > a$ at $p_\parallel < m\sqrt{\alpha q/\rho} - \hbar q/2$, which for $p^2_\parallel/2m = 100$ neV corresponds to $q > p^2_\parallel\rho/m^2\alpha \approx 8\times10^4\ \text{cm}^{-1}$ and $\hbar\omega_q > 23$ neV.

$\varepsilon \approx \mathbf{p}_\parallel^2/2m$, and the final total energy is

$$\varepsilon' = \frac{p_\parallel^2 + p_q^2 - 2p_q p_\parallel \cos\phi}{2m} + E_n + \hbar\omega_q.$$

The replacement $N_q \to N_q + 1$ in Eq. (37) is not important, because for ripplon emission $N_q > K/k_B T \gg 1$. The matrix element is given by Eq. (32). The integration over $\mathbf{p}'$ and over the angle ϕ between $\mathbf{p}_\parallel$ and $\mathbf{p}_q$ is similar to that in Eq. (41) and gives for the rate $w_{\rm em}$ of ripplon emission

$$w_{\rm em} = \int_0^{p_{\rm em}^{\max}} \frac{S N_q p_q dp_q}{\pi\hbar^3} \sum_n \frac{\left|\psi_\perp(0)\psi_\perp'^*(0) V_0 \xi_{0q}\right|^2}{\sqrt{a^2 - (b_1 + \Delta E_n)^2}}, \quad (44)$$

where $a \equiv p_\parallel p_q/m$ as in the previous subsection, and $b_1 = \hbar\omega_q + p_q^2/2m$. The integrand is real when $0 \leqslant \Delta E_n \approx E_n \leqslant a - b_1$. This can be satisfied when $a - b_1 > 0$, which for $p_\parallel^2/2m = 100$ neV gives $p_q < p_{\rm em}^{\max} = \hbar q_{\rm em}^{\max}$ with $q_{\rm em}^{\max} \approx 6.5 \times 10^4$ cm^{-1}. The maximum value of $a - b_1$ is $\sim$3 neV $\ll V_0 = 18.5$ neV. Hence, for the emission of ripplons, $E_n \ll V_0$, and we may use Eqs. (9), (10), and (D18). In addition, instead of three intervals of parameters for the ripplon absorption, we only need to consider one interval. Substituting Eqs. (23), (24) and an upper bound of $|\psi_\perp'(0)|^2 \leqslant |\psi_{\perp 0}(0)|^2$ to Eq. (44), also changing the variable according to Eq. (D18), we obtain an upper bound $w_{\rm em}^{\rm up}$ for $w_{\rm em}$:

$$w_{\rm em}^{\rm up} \approx \int \frac{k_B T dp_q}{\pi^2\hbar^2\alpha p_q} \frac{\left|\psi_{\perp 0}^2(0) V_0\right|^2}{g\sqrt{2m}} \int_0^{a-b_1} \frac{\sqrt{E_n} dE_n}{\sqrt{a^2 - (b_1 + E_n)^2}}. \quad (45)$$

This integral resembles the one in Eq. (D19): the only difference is the sign of E_n in the denominator and, consequently, a different upper integration limit. We may give an upper bound to this integral over E_n by replacing $\sqrt{E_n}$ by its maximum value $\sqrt{a - b_1}$ in the integrand and by replacing the lower limit by $-b_1$, which gives

$$w_{\rm em}^{\rm up} \approx \int_0^{p_{\rm em}^{\max}} \frac{k_B T dp_q}{\pi\hbar^2\alpha p_q} \frac{\left|\psi_{\perp 0}^2(0) V_0\right|^2}{2g\sqrt{2m}} \sqrt{\frac{p_\parallel p_q}{m} - \hbar\omega_q - \frac{p_q^2}{2m}}.$$

This integral converges. Neglecting $p_q^2/2m \ll \hbar\omega_q$ and changing the integration variable to $\sqrt{p_q}$ we finally obtain

$$w_{\rm em}^{\rm up} \approx \frac{k_B T}{\pi\hbar^2\alpha} \frac{\left|\psi_{\perp 0}^2(0) V_0\right|^2}{g\sqrt{2m}} \frac{2}{3} \left(\frac{p_\parallel}{m}\right)^{3/2} \sqrt{\frac{\rho\hbar}{\alpha}}. \quad (46)$$

The rate of ripplon emission depends on the initial neutron momentum $p_\parallel$. At $K = p_\parallel^2/2m = 100$ neV Eq. (46) gives

$$w_{\rm em}^{\rm up} \approx 2 \times 10^{-5}\ {\rm s}^{-1} \times T[{\rm K}]. \quad (47)$$

Combining Eqs. (43) and (47) we obtain an upper bound for the total scattering rate of a surface neutron in the lowest energy level E_0 by ripplons:

$$w_{\rm rip}^{\rm up} = w_{\rm abs}^{\rm up} + w_{\rm em}^{\rm up} \approx 9 \times 10^{-5}\ {\rm s}^{-1} \times T[{\rm K}]. \quad (48)$$

This rate corresponds to a mean neutron scattering time due to the ripplons of $\tau_{\rm rip} > 3$ h even at $T = 1$ K.

V. OTHER NEUTRON SCATTERING PROCESSES

The scattering of ultracold neutrons inside superfluid helium by bulk phonons has been studied in Ref. [46]. There, two main processes were identified: (i) one-phonon absorption and (ii) one-phonon absorption combined with emission of another phonon due to the cubic term in the phonon Hamiltonian. The second process was found to dominate at low temperature, resulting in a total scattering time of about $\tau_{\rm ph0} = 100$ s for a neutron propagating through liquid ^{4}He at $T = 1$ K. In our case both scattering processes are weakened by the factor

$$\int_{-\infty}^0 \psi_\perp^2(z) dz = \psi_\perp^2(0)/2\kappa \approx 1.16 \times 10^{-7},$$

because only a small part of the neutron wave function penetrates into the liquid helium. Hence, for helium temperatures below 1 K, the neutron scattering time constant due to bulk phonons, $\tau_{\rm ph} \approx \tau_{\rm ph0} 2\kappa/\psi_\perp^2(0) \gtrsim 10^9$ s, is extremely long and can safely be ignored.

Recently, another type of surface excitation was proposed semiphenomenologically [47]. These excitations, called surfons, can be considered as ^{4}He atoms in a quasistationary discrete quantum energy level above the liquid ^{4}He surface [47–49], which is somewhat similar to Andreev states [50] of ^{3}He atoms above liquid ^{4}He. Surfons may affect surface electrons [51,52], but so far they received neither direct experimental confirmation, nor substantiation from the numerical calculations [53] of excitations inside liquid ^{4}He. As compared to the vapor-neutron interaction, the surfon-neutron interaction contains an additional small factor $\sim z_0 \psi_\perp^2(0) \sim 3 \times 10^{-5}$ due to the small overlap of the neutron and the surfon wave functions. In addition, at low temperature, $T \lesssim 0.6$ K, the neutron scattering on surfons becomes suppressed exponentially, because of the finite surfon activation energy $\Delta_{s0} \approx k_B \times 2$ K [48], while the ripplons are gapless. Therefore, at any temperature the contribution to neutron scattering rate $w_{\rm sur}$ from surfons is much less than the scattering rate either on He vapor or on ripplons, as can be checked by direct calculation (see Ref. [54] for details):

$$w_{\rm sur} \lesssim \frac{(M k_B T)^{3/2} a_{\rm He}^2}{\hbar^2 m} \left|\psi_{\perp 0}^2(0)\right| \frac{\sqrt{1.6\pi}}{5} \exp\left(\frac{-\Delta_{s0}}{k_B T}\right)$$
$$\approx 4 \times 10^{-8} \exp\left(\frac{-\Delta_{s0}}{k_B T}\right) \times T^{3/2}[{\rm K}]\ {\rm s}^{-1}. \quad (49)$$

Hence, the total scattering rate $w_{\rm tot}$ of UCNs on the liquid helium surface is determined by the helium vapor at high temperatures $T \gtrsim 0.65$ K, and by ripplons at low temperatures $T \lesssim 0.65$ K. It is plotted as function of temperature in Figs. 2 and 3.

VI. SKETCHES OF EXPERIMENTAL IMPLEMENTATIONS, SUMMARY, AND DISCUSSION

The main motivation for the theoretical work presented in this paper is the perspective to perform a high-precision study of the level scheme of the neutron in the gravitational potential above a large liquid mirror. This gives access to short-range, gravitation-like interactions between the neutron

and the mirror currently investigated with comparatively small solid mirrors. In this section we sketch some of the experimental techniques to be developed to take full advantage of a large liquid surface for advancing this study. The system might also serve for detection of tiny energy transfers due to helium-intrinsic or external perturbations. The practical implementation is in line with current work on new UCN sources at the ILL [55–57] which involves cooling many liters of ultrapure, superfluid helium below 0.7 K. This development had been started at the TU Munich [58,59] and builds on theoretical work by Golub and Pendlebury on superthermal UCN production via down-scattering of cold neutrons in superfluid helium [60,61].

An important point to be addressed concerns the population and detection of the neutron quantum states above a superfluid-helium mirror (called the "lake" in what follows), noting that one has to confine the liquid and cope with a meniscus at the border of the container. In the traditional "flow-through" scheme of current experiments the neutrons enter a mirror table with an absorbing ceiling from one side and are detected on the other side. For a liquid mirror, neutrons will then have to enter and exit the lake through a thin, weakly absorbing foil with low (or negative) neutron optical potential. As an alternative method we propose to take advantage of magnetic field gradients for deceleration of neutrons approaching the horizontal mirror located at $z = 0$. Neutrons with magnetic moment μ_n in a magnetic field with modulus B have a potential energy of $\pm|\mu_n|B$, with sign depending on the spin state with respect to the field direction. The upper (lower) sign refers to those neutrons which become repelled (attracted) by a positive gradient of magnetic field modulus. They are correspondingly called low-field (high-field) seekers. Note recent experimental demonstrations of trapped high-field seeking UCNs [62,63]. A magnetic field modulus $B(z) = Cz$, for instance with constant gradient $C > mg/|\mu_n| \approx 1.66\,\mathrm{T/m}$ overcompensates gravitation for the high-field seeking neutrons. Those with vertical kinetic energy $E_\perp = (|\mu_n|C - mg)h$ at height h will thus be slowed down completely when arriving at the mirror. This situation is analog to a neutron rising in the earth's gravitational field to its apogee. If, alternatively, we want to decelerate the low-field seeking neutrons, the gradient has to be inverted, and hence the strongest field needs to be located at the surface. While the neutron is close to the lowest point of its trajectory, the magnetic field gradient nearby the mirror needs to be switched off. A vertical, straight neutron guide ending closely above the mirror will limit the spatial region where the fields need to be provided. Quantum states may be prepared using a circular absorber with a central hole for the neutron-feeding pipe and mounted with variable distance of some tens of μm above the lake. An obvious benefit of the magnetic population method is a possible neutron detection acceptance angle over the full range of 2π.

Compared with a flow-through experiment, the sensitivity of the energy state determination may be drastically improved using lateral UCN trapping prior to detection, ideally for many hundreds of seconds. A multipolar magnetic field, much wider than the system described in Ref. [64] and oriented vertically, may keep low-field seeking neutrons away from the liquid meniscus at the container wall without modification of the vertical neutron state. To populate the lake with high-field seeking neutrons, their spin has to be flipped after arrival at the surface and prior to their arrival in the region of strong multipolar field. This can be done using standard magnetic resonance techniques. Neutrons can still be detected through the side walls of the helium container, requiring switching-off of the magnetic fields (or a spin flip to turn the trapped low-field seeking neutrons into high-field seekers to accelerate them through gaps in the magnetic fence). Alternatively, we may let them rise back to the entrance of the neutron guide by switching on again the magnetic field gradient used for lake population.

Next, we discuss a possible further improvement of the lake population technique sketched above. Note first that in a straight guide most of the neutrons will perform many reflections on their way to the lake. Even a small nonspecularity in the reflection may then become an issue. Much better conditions can be provided using a nonimaging neutron optical device proposed by Hickerson and Filippone [65]. They describe a compound parabolic concentrator (CPC) for neutrons rising from a Lambertian horizontal disk source upwards against the gravitational field. Its neutron-optical properties are based on the "neutron fountain" [66] valid for constant force fields along the symmetry axis of a parabolic reflecting surface. Using the aforementioned constant magnetic field gradient for lake population, neutrons will approach the surface with a constant deceleration $a = C/m - g$. We may thus apply the CPC inverted in space with the neutron source (an aperture with radius R) located at height h above the lake (replacing the straight neutron guide of the scheme discussed before). According to the formulas given in Ref. [65], neutrons starting there at time $t = 0$ and with speed v_0 will, after a time $T = v_R/a$ (where $v_R = \sqrt{v_0^2 + 2aR}$) and with typically fewer than two reflections, arrive within a narrow band of heights $0 \leqslant z < R$ above the horizontal mirror. The spread of total kinetic energy within the ensemble of UCNs is then only $\Delta E \approx maR/3$ and independent of v_0. After switching off the field gradient, the neutrons close to the mirror will thus move with much reduced velocities compared to the traditional beam method. Hence even without lateral trapping, state population via a CPC will increase the time during which the neutron interacts with the mirror and lead to a corresponding gain in accuracy. A CPC will be most beneficial at a pulsed UCN source, preferably in combination with a rebunching technique as demonstrated in Ref. [67], which therefore works best in combination with UCN trapping. We note that the very low lateral neutron velocities allow for quite modest magnetic trapping fields, which makes it easy to provide large openings for neutron detection in the magnetic fence. Obviously, a CPC might also be used for a sufficiently large conventional mirror.

Further investigations are needed to clarify possibilities of neutron manipulation in the presence of a liquid surface. An interesting question is if one can induce transitions, in a controllable way, between levels by vibration of the helium surface. Further possibilities to create a flat mirror of large surface should be investigated as well, such as "Fomblin" oil (a fluorinated, organic compound with low neutron absorption, already tested as part of an optical system

for a new measurement of neutron charge [68]), or liquid or solid neon.

To summarize the theoretical work presented in this paper, we have calculated the temperature-dependent rates of scattering of neutrons propagating in low gravitationally bound states above a neutron optical mirror of superfluid helium. Below about 0.8 K the scattering rate becomes smaller than the neutron β-decay rate. This finding is encouraging for using such a system in studies of the quantum states sketched in Fig. 1. The effect that dominates down to about 0.65 K is scattering by vapor atoms, whereas at lower temperatures interactions with ripplons take over, as was shown in Figs. 2 and 3. Other processes such as neutron interaction with bulk phonons or with surfons turned out to be negligibly small.

The reason why the neutron-ripplon scattering becomes dominant at lowest temperatures is the linear temperature dependence of this effect [see Eq. (48)]. Since at 0.6 K the scattering rate is already 50 times smaller than the neutron decay rate, it will be completely insignificant for precision studies of the level scheme. When considering neutron lifetime measurements using the storage of UCNs by the neutron optical potential of liquid helium [69,70], however, the scattering rate cannot be neglected. What is helpful is that the main contribution to the scattering rate is due to the low-energy part of the ripplon spectrum, where the dominant energy transfers will be only a few peV. Such transfers are usually insufficient to cause a neutron to penetrate through the liquid helium and thus leave the system. At 0.6 K, therefore, the mean escape time of a UCN with initial kinetic energy $K < V_0$ could be longer than the neutron β-decay lifetime by several orders of magnitude. For highest reliability the neutron spectrum should be prepared with a gap between its upper cut-off and V_0. It should also be noted that the value $V_0 = 18.5$ neV for superfluid helium is small compared to $\gtrsim$100 neV for conventional materials used for neutron bottles. Counting statistics might therefore become a limiting issue. Nonetheless, a neutron lifetime measurement employing a trap involving a horizontal surface of superfluid helium seems an interesting complement to projects employing magnetic neutron traps. While these possess typical trapping potentials for low-field-seeking neutrons in the range (50–120) neV and completely avoid wall collisions of truly trapped neutrons, other systematic effects such as marginally trapped neutrons and depolarization need to be carefully addressed [71–78]. We note Refs. [79,80] for recent reviews and discussion of the neutron lifetime problem.

ACKNOWLEDGMENTS

P.G. thanks A. M. Dyugaev and A.G. thanks A. F. Krutov for useful discussions. The work was partially supported by Russian Foundation for Basic Research Grant No. 16-02-00522.

APPENDIX A: MATRIX ELEMENTS OF THE INTERACTION BETWEEN A NEUTRON AND HE VAPOR ATOM

The initial neutron wave function is given by Eqs. (4), (5), and (7). Since the typical neutron out-of-plane kinetic energy after scattering by a He atom of the vapor is much larger than E_0, and mostly even larger than V_0 given in Eq. (2), the final neutron wave function is close to the three-dimensional plane wave with momentum $\mathbf{p}'$, normalized to one particle in the whole volume V:

$$\psi' = \exp(i\mathbf{p}'\mathbf{r}/\hbar)/\sqrt{V}. \tag{A1}$$

The initial He-atom wave function is $\Psi = \exp(i\mathbf{P}\mathbf{r}/\hbar)$, and the final He wave function is $\Psi' = \exp(i\mathbf{P}'\mathbf{r}/\hbar)$. The matrix element of the interaction potential (1) is given by

$$\begin{aligned} T_{if} &= \int d^3\mathbf{r}\, \psi_{\perp 0}(z)\psi_{\parallel}(\mathbf{r}_{||})\psi'(\mathbf{r}) \\ &\quad \times \int d^3\mathbf{R} \exp\left(\frac{i(\mathbf{P}-\mathbf{P}')\mathbf{R}}{\hbar}\right) U\, \delta^{(3)}(\mathbf{r}-\mathbf{R}) \\ &= U \int \frac{d^3\mathbf{R}}{\sqrt{SV}} \psi_{\perp 0}(z_{\mathrm{He}}) \exp\left(\frac{i\Delta\mathbf{P}_{\mathrm{tot}}\mathbf{R}}{\hbar}\right), \end{aligned} \tag{A2}$$

where $\Delta\mathbf{P}_{\mathrm{tot}} \approx \mathbf{P} - \mathbf{P}' + \mathbf{p}_{||} - \mathbf{p}'$ is the change of total momentum, $\mathbf{R}$ is the coordinate of the He nucleus, and $\psi_{\perp 0}(z) = C_0\,\mathrm{Ai}[(z - E_0/mg)/z_0]$ according to Eq. (7). Introducing $\tilde{u} \equiv z/z_0$ and performing the integration over $d^2\mathbf{R}_{\parallel}$ in Eq. (A2) using the identity

$$\int d^2\mathbf{R}_{\parallel} \exp(i\Delta\mathbf{P}_{\mathrm{tot}\parallel}\mathbf{R}_{\parallel}/\hbar) = (2\pi\hbar)^2\delta^{(2)}(\Delta\mathbf{P}_{\mathrm{tot}||}), \tag{A3}$$

one can rewrite T_{if} as

$$T_{if} = \frac{U\,(2\pi\hbar)^2\delta^{(2)}(\Delta\mathbf{P}_{\mathrm{tot}||})}{\sqrt{SV/z_0}} I, \tag{A4}$$

where the remaining integral is

$$I \equiv 1.4261 \int_0^{\infty} d\tilde{u}\ \mathrm{Ai}(\tilde{u} - \alpha_1) \exp\left(\frac{i\Delta p_z \tilde{u}}{\hbar/z_0}\right).$$

We calculate this integral approximately by replacing the normalized Airy function $f(\tilde{u}) \equiv 1.4261\mathrm{Ai}(\tilde{u} - \alpha_1)$ by a simpler form, also normalized, that is a close approximation, i.e., $f(\tilde{u}) \approx \exp[-(\tilde{u} - \tilde{u}_0)^2/2]/\pi^{1/4}$, where $\tilde{u}_0 \approx 1.5$. Then,

$$\begin{aligned} I &= \int_0^{\infty} d\tilde{u}\ f(\tilde{u}) \exp\left(\frac{i\Delta p_z \tilde{u}}{\hbar/z_0}\right) \\ &\approx \pi^{1/4}\sqrt{2} \exp\left[\frac{i\Delta p_z \tilde{u}_0}{\hbar/z_0} - \frac{1}{2}\left(\frac{\Delta p_z}{\hbar/z_0}\right)^2\right]. \end{aligned} \tag{A5}$$

Below we need only the square of the absolute value of the matrix element T_{if}. The square of the δ function in $|T_{if}|^2$ should be treated as

$$[(2\pi\hbar)^2\delta^{(2)}(\Delta\mathbf{P}_{\mathrm{tot}||})]^2 = S(2\pi\hbar)^2\delta^{(2)}(\Delta\mathbf{P}_{\mathrm{tot}||}), \tag{A6}$$

because it comes from the extra integration over the coordinate $\mathbf{r}_{i||}$: $\int d^2\mathbf{r}_{i\parallel} = S$. Indeed, substituting Eq. (A3) to the left-hand side of Eq. (A6) we obtain

$$\begin{aligned} &(2\pi\hbar)^2\delta^{(2)}(\Delta\mathbf{P}_{\mathrm{tot}||}) \int d^2\mathbf{r}_{i\parallel} \exp\left(\frac{i\Delta\mathbf{P}_{\mathrm{tot}\parallel}\mathbf{r}_{i\parallel}}{\hbar}\right) \\ &= (2\pi\hbar)^2\delta^{(2)}(\Delta\mathbf{P}_{\mathrm{tot}||}) \int d^2\mathbf{r}_{i\parallel} = S(2\pi\hbar)^2\delta^{(2)}(\Delta\mathbf{P}_{\mathrm{tot}||}). \end{aligned}$$

Substituting Eq. (A5) to Eq. (A4) and using Eq. (A6), we obtain

$$|T_{if}|^2 \approx \frac{U^2\,(2\pi\hbar)^3\delta^{(2)}(\Delta\mathbf{P}_{\mathrm{tot}||})}{V\sqrt{\pi}\hbar/z_0}\exp\left[-\left(\frac{\Delta p_z}{\hbar/z_0}\right)^2\right].$$

Since $\hbar/z_0 \ll P$, using the identity

$$\delta(x) = \lim_{\epsilon\to 0}\left[\frac{1}{\epsilon\sqrt{\pi}}\exp\left(-\frac{x^2}{\epsilon^2}\right)\right],$$

we obtain Eq. (11) for $|T_{if}|^2$.

APPENDIX B: DERIVATION OF THE NEUTRON-RIPPLON INTERACTION IN THE ADIABATIC APPROXIMATION

The Schrödinger equation for a neutron is given by

$$\hat{H}\psi(\mathbf{r},t) = i\hbar\partial\psi(\mathbf{r},t)/\partial t, \tag{B1}$$

where the Hamiltonian

$$\hat{H} = \hat{K} + \hat{V} = -\frac{\hbar^2\hat{\Delta}}{2m} + mgz + V_0\theta[-z+\xi(\mathbf{r}_\parallel,t)] \tag{B2}$$

contains the neutron kinetic energy $\hat{K} = -\hbar^2\hat{\Delta}/2m$ and the potential energy $\hat{V} = mgz + V_0\theta[-z+\xi(\mathbf{r}_\parallel,t)]$. The latter contains the effects of the Earth's gravitational field and the potential wall due to the liquid helium, as shown in Fig. 1. The difference from Eq. (3) is that the liquid helium has now a time- and space-periodic boundary $\xi(\mathbf{r}_\parallel,t)$ given by Eq. (20). The difference between Eq. (B2) and Eq. (4) from Ref. [28] is that the surface has now a periodic spatial dependence.

The adiabatic adjustment of the neutron wave function to the new surface profile means that the neutron wave function, in first approximation, adiabatically shifts in z direction by the length $\xi(\mathbf{r}_\parallel,t)$: $\psi(\mathbf{r},t) \to \tilde{\psi}(\mathbf{r}+\xi(\mathbf{r}_\parallel,t)\hat{\mathbf{z}},t)$, where $\hat{\mathbf{z}}$ is the unitary vector in z direction. This shift can be written via the translation (z-shift) operator

$$\hat{T}_z(\xi) = \exp[\xi(\mathbf{r}_\parallel,t)\partial/\partial z] = \exp[i\xi(\mathbf{r}_\parallel,t)p_z/\hbar].$$

Its action on the wave function is

$$\hat{T}_z(\xi)\psi_\perp(z) = \psi_\perp(z+\xi).$$

We also define a new wave function

$$\tilde{\psi}(\mathbf{r}+\xi\hat{\mathbf{z}},t) = \psi(\mathbf{r},t) = \hat{T}_z(\xi)\tilde{\psi}(\mathbf{r},t),$$

which after substitution into Eq. (B1) gives a new Schrödinger equation for $\tilde{\psi}(\mathbf{r},t)$:

$$\hat{H}\hat{T}_z(\xi)\tilde{\psi}(\mathbf{r},t) = i\hbar\partial(\hat{T}_z(\xi)\tilde{\psi}(\mathbf{r},t))/\partial t. \tag{B3}$$

The action of the shift operator on the potential energy function $V(\mathbf{r})$ is given by

$$V(\mathbf{r})\hat{T}_z(\xi) = \hat{T}_z(\xi)V(\mathbf{r}-\xi(\mathbf{r}_\parallel,t)\hat{\mathbf{z}}), \tag{B4}$$

while for the commutator with kinetic-energy operator $\hat{K} = -\hbar^2\hat{\Delta}/2m$ we have

$$\begin{aligned}\hat{K}\hat{T}_z(\xi) - \hat{T}_z(\xi)\hat{K} &= -\frac{\hbar^2}{m}(\nabla^2 e^{\xi(\mathbf{r}_\parallel,t)\partial/\partial z} - e^{\xi(\mathbf{r}_\parallel,t)\partial/\partial z}\nabla^2)\\ &= \frac{2\hat{p}_\parallel\hat{p}_q + \hat{p}_q^2}{2m}\xi(\mathbf{r}_\parallel,t)\frac{\partial}{\partial z}\\ &= \frac{(\hat{p}_\parallel+\hat{p}_q)^2 - \hat{p}_\parallel^2}{2m}\xi(\mathbf{r}_\parallel,t)\frac{\partial}{\partial z},\end{aligned} \tag{B5}$$

where $\hat{p}_\parallel = -i\hbar\nabla_\parallel$ and $\hat{p}_q = \hbar q$ are the neutron and the ripplon momentum operators along the surface, respectively. The time-dependence of $\xi(\mathbf{r}_\parallel,t)$ also gives an additional term on the right-hand side of Eq. (B3):

$$\begin{aligned}i\hbar\frac{\partial}{\partial t}(\hat{T}_z\tilde{\psi}(\mathbf{r},t)) &= i\hbar\frac{\hat{T}_z\partial\tilde{\psi}(\mathbf{r},t)}{\partial t} + i\hbar\frac{\partial\hat{T}_z}{\partial t}\tilde{\psi}(\mathbf{r},t)\\ &= i\hbar\frac{\hat{T}_z\partial\tilde{\psi}(\mathbf{r},t)}{\partial t} + \hbar\omega_q\xi(\mathbf{r}_\parallel,t)\frac{\partial}{\partial z}\hat{T}_z\tilde{\psi}(\mathbf{r},t).\end{aligned} \tag{B6}$$

Combining Eqs. (B3) and (B6) we obtain a new Schrödinger equation,

$$\hat{T}_z\{\hat{H}_0 + \hat{H}_{\mathrm{int}} - i\hbar\partial/\partial t\}\tilde{\psi}(\mathbf{r},t) = 0, \tag{B7}$$

where $\hat{H}_0$ is given by Eq. (3) and the interaction term is given by

$$\hat{H}_{\mathrm{int}} = \xi(\mathbf{r}_\parallel,t)\left\{\left[\frac{2\hat{p}_\parallel\hat{p}_q + \hat{p}_q^2}{2m} - \hbar\omega_q\right]\frac{\partial}{\partial z} + mg\right\}. \tag{B8}$$

APPENDIX C: CROSSOVER BETWEEN ADIABATIC AND DIABATIC LIMITS IN CLASSICAL PHYSICS

For a classical particle above the surface in the limit $V_0 \to \infty$ the crossover between diabatic and adiabatic limits occurs when the maximal acceleration of the helium surface $\partial^2\xi_q/\partial t^2 = \omega_q^2\xi_q$, due to its oscillatory motion, becomes equal to the free fall acceleration g,

$$\omega_{qc}^2\xi_q = g. \tag{C1}$$

The classical amplitude ξ_q of the surface oscillations with wave vector $\mathbf{q}$ differs from ξ_{0q} in Eq. (24) by the square root of the Bose distribution function N_q given by Eq. (38):[4]

$$\xi_q = \sqrt{N_q}\xi_{0q} \approx \xi_{0q}\sqrt{k_{\mathrm{B}}T/\hbar\omega_q}. \tag{C2}$$

In addition, ξ_{0q} in Eq. (24) depends on the surface S, which must be defined. In the formulas for the neutron scattering rate by ripplons this surface-dependence is unphysical and does not occur explicitly, because the S dependence of the ripplon amplitude in Eq. (24) is compensated by the S dependence of the ripplon density of states (see below). Similarly, the total mean square amplitude of thermal surface oscillations at any point $r_\parallel$ is given by the sum over all $\mathbf{q}$ vectors,

$$\langle\xi^2(r_\parallel)\rangle = \sum_{\mathbf{q}}\xi_{\mathbf{q}}^2 = \int N_q\xi_{0\mathbf{q}}^2\frac{Sd^2\mathbf{q}}{(2\pi)^2},$$

and the surface area S drops out. More generally, if we are interested in the surface waves with the wave number q in some interval $\Delta q_x\Delta q_y$, then we sum all ripplon modes in the phase volume $S\Delta q_x\Delta q_y$, and the surface area S again drops out from the total $\langle\xi^2\rangle$. In the estimate (C1) for the adiabatic-diabatic

[4]The thermally excited ripplons are not coherent, therefore the population factor N_q increases the mean energy of the surface wave by N_q times, not the amplitude of thermal ripplons, which is increased only by $\sqrt{N_q}$ times.

crossover the surface S is defined by the area S_n of the neutron wave function along the surface, which corresponds to the momentum smearing $\Delta q_x \Delta q_y \sim S_n^{-1}$.

For a lower estimate of the classical crossover frequency ω_{qc}, we take the minimal possible S given by the square of the wave length: $S_{\min} \approx (2\pi/q)^2$. Then, substituting it to Eq. (24), we have

$$\xi_{0q}^{\max} \approx \left(\frac{\hbar q^2}{8\pi^2\sqrt{\rho\alpha q}}\right)^{1/2} = \frac{q^{3/4}}{2\pi}\left(\frac{\hbar/2}{\sqrt{\rho\alpha}}\right)^{1/2}. \tag{C3}$$

For $q = 1\ \mu\text{m}^{-1} = 10^4\ \text{cm}^{-1}$ this formula gives $\xi_{0q}^{\max} \approx 7 \times 10^{-5}$ nm, which is much less than q^{-1}. The corresponding

$$\xi_q^{\max} \approx \xi_{0q}^{\max}\sqrt{\frac{k_B T}{\hbar\omega_q}} = \frac{1}{2\pi}\left(\frac{k_B T}{2\alpha}\right)^{1/2} \approx 0.02\ \text{nm}\sqrt{T\ [\text{K}]} \tag{C4}$$

is also much less than q^{-1}, and we can apply the usual surface wave description. Substituting $S_{\min} \approx (2\pi/q)^2$ to Eqs. (24), (C1), and (38) gives

$$g = \omega_{qc}^{3/2}\left(\frac{k_B T\, q^{3/2}}{2(2\pi)^2\sqrt{\rho\alpha}}\right)^{1/2},$$

which, using Eq. (23), gives the lowest estimate for the crossover frequency

$$\omega_{qc} = \sqrt{2\pi g\sqrt{\frac{2\alpha}{k_B T}}} \approx \frac{6.6 \times 10^5\ \text{s}^{-1}}{(T\ [\text{K}])^{1/4}}. \tag{C5}$$

This frequency corresponds to the neutron energy (at $T = 1$ K) $\hbar\omega_{qc} \approx 7 \times 10^{-22}$ erg ≈ 0.44 neV $> E_0$ and to

$$q_c = 0.56\ \mu\text{m}^{-1} > \varkappa. \tag{C6}$$

Hence, in the diabatic limit $q > q_c$, and we can always use the ripplon dispersion given by Eq. (23).

Another condition of the classical adiabatic limit is that the curvature of the surface $\nabla^2\xi = q^2\xi_q^{\max}$ is less than the curvature of the neutron trajectory due to the parabolic free-fall motion $\partial^2 z/\partial r_\parallel^2 = g/v_\parallel^2$, where $v_\parallel$ is the neutron velocity along the surface. Taking a UCN kinetic energy of $K_\parallel = 100$ neV, corresponding to $v_\parallel^2 = 2K_\parallel/m = 19\ \text{m}^2/\text{s}^2$, we can check that the condition $q^2\xi_q^{\max} < g/v_\parallel^2$ is fulfilled at $q = q_c = 0.56\ \mu\text{m}^{-1}$. Hence, the condition $\omega_q < \omega_{qc}$ given by Eq. (C5) ensures the classical adiabatic limit.

APPENDIX D: CALCULATIONS FOR THE NEUTRON SCATTERING RATE DUE TO RIPPLON ABSORPTION

In this section we evaluate the integral in Eq. (41) or (42), which gives the neutron scattering rate by ripplons. The integration over p_q and n in Eq. (41) can be separated into several regions, given by different limits of the ratio $p_q/p_\parallel$ and of the difference $\Delta E_n - V_0$. For $\Delta E_n < V_0$ the final neutron vertical state belongs to a discrete energy spectrum, approximately given by Eq. (9). For $\Delta E_n > V_0$ the final neutron vertical state belongs to the continuous energy spectrum and can approximately be taken as a plane wave.

In the region $p_q \gg p_\parallel$ the initial neutron kinetic energy is negligible and, for the majority of the scattering events, the change of the neutron out-of-plane kinetic energy $\Delta E_n > V_0$. The integral in Eq. (41) is evaluated in this limit in Appendix D1 below.

In the region of small ripplon momentum, $p_q \lesssim p_\parallel$, studied in Appendix D2, the angle ϕ between the initial neutron and ripplon momenta is important for the out-of-plane energy transfer ΔE_n, and the scattering rate depends on the initial neutron momentum $p_\parallel$. Depending on the sign of the difference $\Delta E_n - V_0$, this region is split into two. For $\Delta E_n < V_0$ the final neutron state belongs to the discrete spectrum and is described by the formulas in Sec. II. For $\Delta E_n > V_0$ the final vertical neutron state belongs to the continuous spectrum and can be approximated by Eqs. (D2) and (D3).

1. Absorption of thermal (high-energy) ripplons

In this subsection we consider the region of large momenta $p_q \gg p_\parallel = \sqrt{2Km}$ contributing to the integral in Eq. (41). The in-plane kinetic energy K of ultracold neutrons is, usually, less than $K_* = 100$ neV, which corresponds to a maximal initial neutron wave number $q_* = p_{\parallel *}/\hbar = 0.07\ \text{nm}^{-1}$ and to a maximal neutron velocity $v_{\parallel *} = \sqrt{2K/m} = 4.4$ m/s. For $q = q_*$ the ripplon energy, according to Eq. (23), is given by

$$\hbar\omega_{q*} \equiv \hbar\omega_q(\hbar q = p_{\parallel *}) \approx 600\ \text{neV} \gg V_0, K_*, \tag{D1}$$

and the ripplon velocity is $v_{q*} = 3\omega_{q*}/2q_* \approx 20$ m/s.[5] If a ripplon with such a high energy is absorbed, the final out-of-plane neutron energy $E_n \sim \hbar\omega_q$ is much higher than the potential barrier $V_0 = 18.5$ neV. It is then reasonable to take the final out-of-plane neutron wave function as a plane wave,

$$\psi_{\perp n}(z) \approx \exp(ip_z' z/\hbar)/\sqrt{L_z}. \tag{D2}$$

Accordingly, the neutron out-of-plane energy can be approximated by the free-particle quadratic dispersion

$$E_n \approx p_z'^2/2m, \tag{D3}$$

where p_z' is the component of the final neutron momentum perpendicular to the surface. The sum over out-of-plane neutron wave number n in Eq. (41) then becomes an integral over p_z':

$$\sum_n \to \int \rho_n(p_z')dp_z', \tag{D4}$$

where the one-dimensional neutron density of states is given by[6]

$$\rho_n(p_z') \approx L_z/2\pi\hbar. \tag{D5}$$

[5]The typical thermal ripplon has even larger energy $\hbar\omega_q \sim k_B T \approx 0.5$ K, corresponding to the wave number $q \approx 1.2\ \text{nm}^{-1}$ and the velocity $v_q \equiv \partial\omega_q/\partial q \approx 82$ m/s.

[6]Equations (D2)–(D4) can also be applied for smaller E_n if $p_z' = p_z'(z)$ is understood as a quasiclassical coordinate-dependent momentum; then in Eq. (D3) one should take its value at $z = 0$, and $\rho_n(p_z')$ differs from Eq. (D5) and depends on the actual spectrum.

For scattering by thermal ripplons with $q > q_*$ the initial neutron energy $K \approx p_\parallel^2/2m$ and momentum $p_\parallel < p_q$ can be neglected. Eqs. (39) and (40) then simplify to

$$\varepsilon \approx \hbar\omega_q; \quad \varepsilon' \approx \left(p_q^2 + p_z'^2\right)/2m. \tag{D6}$$

Using Eq. (22), we rewrite Eq. (41) as (the lower index ">" means large ripplon energy):

$$\begin{aligned} w_> &= \int_{\hbar q_*}^{\infty} \frac{\hbar|\psi_{\perp 0}(0)V_0|^2}{2\sqrt{\rho\alpha q}} \frac{N_q p_q dp_q}{2\pi\hbar^2} \\ &\times \int_0^{\infty} \frac{dp_z'}{\hbar^2} \delta\left(\hbar\omega_q - \frac{p_q^2 + p_z'^2}{2m}\right) \\ &= \int_{q_*}^{\infty} \frac{|\psi_{\perp 0}(0)V_0|^2}{2\pi\hbar\sqrt{\rho\alpha}} \frac{mN_q\sqrt{q}dq}{\sqrt{2m\hbar\omega_q - \hbar^2 q^2}}. \end{aligned} \tag{D7}$$

The square root in the denominator is real at $2m\hbar\omega_q = 2m\hbar\sqrt{\alpha/\rho}q^{3/2} > \hbar^2 q^2$, which gives $q < 4q_0 \equiv (2m/\hbar)^2\alpha/\rho \approx 2.5$ nm^{-1} and corresponds to the ripplon energy $\hbar\omega_q < \hbar\omega_{q\,\max} \approx \hbar(2m/\hbar)^3(\alpha/\rho)^2 = 2\times 10^{-16}$ erg $\approx k_B \times 1.5$ K $\gtrsim k_B T$. Above this energy the simple absorption of a ripplon by a UCN in a surface state is impossible because of the conservation laws for energy and momentum. Substituting Eqs. (23) and (38) to Eq. (D7), and introducing the dimensionless variable $\zeta \equiv \hbar\omega_q/k_B T$, for which $q = (\zeta k_B T\sqrt{\rho/\alpha}/\hbar)^{2/3}$, we obtain

$$w_> = \frac{|\psi_{\perp 0}(0)V_0|^2\sqrt{mk_B T}}{3\pi\hbar^2\alpha\sqrt{2}} \int_{\zeta_{\min}}^{\zeta_{\max}} \frac{\zeta^{-1/2}d\zeta(e^\zeta - 1)^{-1}}{\sqrt{1-(\zeta/\zeta_{\max})^{1/3}}}, \tag{D8}$$

where $\zeta_{\min} = \hbar\omega_{q*}/k_B T$ is given by Eq. (D1) and $\zeta_{\max} = \hbar\omega_{q\,\max}/k_B T = (2m)^3(\alpha/\hbar\rho)^2/k_B T \sim 1$. The integration in Eq. (D8) diverges as $\zeta_{\min}^{-1/2}$ at the lower limit, and the main part of the integral comes from this divergence:

$$w_> \approx \frac{|\psi_{\perp 0}(0)V_0|^2\sqrt{mk_B T}}{3\pi\hbar^2\alpha\sqrt{2}\sqrt{\zeta_{\min}}}. \tag{D9}$$

Substituting the cutoff $\zeta_{\min} = \hbar\omega_{q*}/k_B T$ given by Eq. (D1) and other numerical values to Eq. (D9), we obtain the contribution to the neutron scattering rate from the high-energy ripplons with $\hbar q > p_{\parallel *}$:

$$w_> \approx 1.7\times 10^{-6}\ \text{s}^{-1} \times T[\text{K}]. \tag{D10}$$

At smaller ripplon energy, i.e., at $\hbar q < p_{\parallel *}$, the integral in Eq. (41) must be estimated without the approximation in Eqs. (D2)–(D6). In the next subsection we show that Eq. (D9) overestimates the integral in Eq. (41) for $\hbar q < p_\parallel$, especially for $\hbar\omega_q \lesssim V_0$ where the infrared divergence disappears.

At $K_* \to 0$, when the cutoff given by $q_* = \hbar/p_{\parallel *}$ is too small, the infrared divergence in Eq. (D9) must be cut off at $\zeta_{\min} \approx V_0/k_B T$, because the approximation given by Eqs. (D2)–(D5) is not valid for lower ripplon energies, for which the neutron state after the absorption still belongs to the discrete spectrum along the z axis. A rough estimate of the absorption rate of high-energy ripplons with $\hbar\omega_q > V_0$ can be obtained for small initial neutron energies $K < V_0$ by substituting $\zeta_{\min} \approx V_0/k_B T$ to Eq. (D9):

$$w_>^{\text{up}} \approx w_>(\zeta_{\min} \approx V_0/k_B T) \approx 10^{-5}\ \text{s}^{-1} \times T[\text{K}]. \tag{D11}$$

This estimate gives a neutron mean scattering time $1/w_>^{\text{up}} \approx 27$ h, which is much greater than the intrinsic neutron lifetime.

2. Upper bound of the absorption rate of low-energy ripplons

For $k_B T \gg \hbar\omega_q$ the ripplon population is given by $N_q \approx k_B T/\hbar\omega_q$. Substituting Eqs. (23) and (24) into Eq. (42) we obtain

$$w_< = \int_0^{p_{\max}} \frac{k_B T dp_q^2}{4\pi\hbar\alpha p_q^2} \sum_n \frac{|\psi_{\perp 0}(0)\psi_{\perp n}^*(0)V_0|^2}{\sqrt{a^2 - (b-E_n)^2}}. \tag{D12}$$

a. Transitions to a continuous neutron spectrum

In this subsection we consider the case of final neutron energies $E_n > V_0$ above the potential barrier and thus belonging to a continuous spectrum. We may then apply the approximation given by Eqs. (D2)–(D5) and rewrite Eq. (D12) as

$$w_< \approx \int_{p_{\min}}^{p_{\max}} \frac{k_B T dp_q^2}{4\pi\hbar\alpha p_q^2} \frac{|\psi_{\perp 0}(0)V_0|^2}{2\pi\hbar} I, \tag{D13}$$

where the integral

$$I \equiv \int \frac{dp_z'}{\sqrt{a^2 - (b - p_z'^2/2m)^2}} = \int_{V_0}^{a+b} \frac{\sqrt{m/2E_n}dE_n}{\sqrt{a^2-(b-E_n)^2}}. \tag{D14}$$

For $b > a$ we may give an upper bound to this integral:

$$I < I_{\max} = \frac{\sqrt{m}}{\sqrt{2V_0}} \int_{b-a}^{b+a} \frac{dE_n}{\sqrt{a^2-(b-E_n)^2}} = \frac{\pi\sqrt{m}}{\sqrt{2V_0}}. \tag{D15}$$

The corresponding upper bound of Eq. (D13) is

$$w_<^{\text{up}} \approx \frac{k_B T|\psi_{\perp 0}(0)V_0|^2\sqrt{m}}{4\pi\hbar^2\alpha\sqrt{2V_0}} \ln\left(\frac{p_{\max}}{p_{\min}}\right). \tag{D16}$$

The interval of integration $V_0 \leqslant E_n \leqslant b + a$ in Eq. (D14) is nonzero for $b + a \approx \hbar\omega_q + p_\parallel p_q/m > V_0$, which for $p_\parallel^2/2m = 100$ neV corresponds to $q > q_{\min} \equiv p_{\min}/\hbar \approx 4\times 10^4$ cm^{-1}. Substituting also $\psi_{\perp 0}(0) \approx 0.236$ cm$^{-1/2}$ and $p_{\max} = p_{\parallel *}$ into Eq. (D16), we obtain

$$w_<^{\text{up}} \approx 7.3\times 10^{-6}\ln(q_*/q_{\min}) \times T[\text{K}] \approx 2\times 10^{-5} \times T[\text{K}]. \tag{D17}$$

b. Transitions to the discrete neutron levels

In this subsection we consider the case of final neutron energies in the interval $0 < \Delta E_n \lesssim V_0$ below the potential barrier and approximately given by Eqs. (9) and (10). Since $V_0 \gg E_0$, the sum over n in Eq. (D12) still includes many terms and can be approximated by an integration over n for $n \gg 1$. Equations (9) and (10) give $E_n \approx mgz_0(3\pi n/2)^{2/3}$, which can be rewritten as

$$n \approx \frac{2}{3\pi}\left(\frac{\Delta E_n}{mgz_0}\right)^{3/2} = \frac{2(\Delta E_n)^{3/2}}{3\pi g\hbar}\sqrt{\frac{2}{m}}$$

and gives

$$\frac{dn}{dE_n} = \frac{\sqrt{E_n}}{\pi g\hbar}\sqrt{\frac{2}{m}}. \tag{D18}$$

We also use that $|\psi^*_{\perp n}(0)| \lesssim \psi_{\perp 0}(0)$, and for an upper estimate of Eq. (D12) we replace $|\psi^*_{\perp n}(0)|$ by $|\psi_{\perp 0}(0)|$ for $E_n < V_0$. Using Eq. (D18), we rewrite Eq. (D12) for $\Delta E_n < V_0$ as

$$w_{\ll} \approx \int_0^{p_{\max}} \frac{k_B T dp_q}{\pi\hbar^2\alpha p_q} \frac{\left|\psi^2_{\perp 0}(0)V_0\right|^2}{\pi g\sqrt{2m}} \int_0^{V_0} \frac{\sqrt{E_n}dE_n}{\sqrt{a^2-(b-E_n)^2}}. \tag{D19}$$

This integral converges, with main contributions from $E_n \sim V_0$. An upper bound $w^{\rm up}_{\ll}$ of this integral can be obtained by replacing $\sqrt{E_n}$ by $\sqrt{V_0}$ in the integrand and by extending the integration region from $(0, V_0)$ to $(a-b, a+b)$. This gives an integral over E_n similar to Eq. (D15):

$$\begin{aligned} w^{\rm up}_{\ll} &= \int_{p_{\min}}^{p_{\max}} \frac{k_B T dp_q}{\pi\hbar^2\alpha p_q} \frac{\left|\psi^2_{\perp 0}(0)V_0\right|^2\sqrt{V_0}}{\pi g\sqrt{2m}} \\ &\quad\times \int_{b-a}^{b+a} \frac{dE_n}{\sqrt{a^2-(b-E_n)^2}} \\ &= \frac{k_B T\left|\psi^2_{\perp 0}(0)V_0\right|^2\sqrt{V_0}}{\pi\hbar^2\alpha g\sqrt{2m}} \ln\left(\frac{p_{\max V0}}{p_{\min V0}}\right). \end{aligned} \tag{D20}$$

Since $V_0 > E_n$ and the integrand in Eq. (D19) is real for $b-a < E_n < b+a$, the region of integration over E_n in Eq. (D19) is nonzero if $b-a \approx \hbar\omega_q - p_\parallel p_q/m < V_0$, which for $p^2_\parallel/2m = 100$ neV corresponds to $p_q < p_{\max} \approx \hbar q_{\max V0}$ with $q_{\max V0} = 1.57\times 10^5$ cm^{-1}. On the other hand, $\Delta E_n < b+a$ can reach V_0 if $b+a \approx \hbar\omega_q + p_\parallel p_q/m \geqslant V_0$. For $p^2_\parallel/2m = 100$ neV this gives $p_q > p_{\min V0} \approx \hbar q_{\min V0}$ with $q_{\min V0} = 3.8\times 10^4$ cm^{-1}. For $p_q < p_{\min V0}$ the logarithmic divergence disappears. Hence, using Eq. (D20) we obtain an upper estimate of $w_{\ll}$:

$$w^{\rm up}_{\ll} \approx 4\times 10^{-5}\times T[\mathrm{K}]\ \mathrm{s}^{-1}. \tag{D21}$$

[1] D. Dubbers and M. G. Schmidt, Rev. Mod. Phys. **83**, 1111 (2011).
[2] M. J. Ramsey-Musolf and S. Su, Phys. Rep. **456**, 1 (2008).
[3] H. Abele, Prog. Nucl. Phys. **60**, 1 (2008).
[4] R. Golub, D. J. Richardson, and S. K. Lamoreaux, *Ultra-Cold Neutrons* (Adam Hilger, Bristol, 1991).
[5] V. K. Ignatovich, *The Physics of Ultracold Neutrons* (Oxford Science Publications, Clarendon Press, Oxford, 1990).
[6] E. M. Purcell and N. F. Ramsey, Phys. Rev. **78**, 807 (1950).
[7] M. Pospelov and A. Ritz, Ann. Phys. (NY) **318**, 119 (2005).
[8] C. A. Baker, D. D. Doyle, P. Geltenbort, K. Green, M. G. D. vanderGrinten, P. G. Harris, P. Iaydjiev, S. N. Ivanov, D. J. R. May, J. M. Pendlebury, J. D. Richardson, D. Shiers, and K. F. Smith, Phys. Rev. Lett. **97**, 131801 (2006).
[9] A. P. Serebrov, E. A. Kolomenskiy, A. N. Pirozhkov *et al.*, Pis'ma v Zh. Eksp. Teor. Fiz. **99**, 7 (2014) [Sov. Phys. JETP Lett. **99**, 4 (2014)].
[10] A. Coc, N. J. Nunes, K. A. Olive, J. P. Uzan, and E. Vangioni, Phys. Rev. D **76**, 023511 (2007).
[11] R. E. Lopez and M. S. Turner, Phys. Rev. D **59**, 103502 (1999).
[12] V. I. Luschikov and A. I. Frank, JETP Lett. **28**, 559 (1978).
[13] V. V. Nesvizhevsky, H. G. Börner, A. K. Petukhov, H. Abele, S. Baessler, F. J. Ruess, T. Stöferle, A. Westphal, A. M. Gagarski, G. A. Petrov, and A. V. Strelkov, Nature (London) **415**, 297 (2002).
[14] V. V. Nesvizhevsky, A. K. Petukhov, H. G. Börner, T. A. Baranova, A. M. Gagarski, G. A. Petrov, K. V. Protasov, A. Y. Voronin, S. Baessler, H. Abele, A. Westphal, and L. Lucovac, Eur. Phys. J. C **40**, 479 (2005).
[15] A. Westphal, H. Abele, S. Baessler, V. Nesvizhevsky, K. Protasov, and A. Voronin, Eur. Phys. J. C **51**, 367 (2007).
[16] N. Arkani-Hamed, S. Dimopoulos, and G. Dvali, Phys. Rev. D **59**, 086004 (1999).
[17] I. Antoniadis, Lect. Notes Phys. **631**, 337 (2003).
[18] P. Brax and G. Pignol, Phys. Rev. Lett. **107**, 111301 (2011).
[19] T. Jenke, G. Cronenberg, J. Burgdörfer, L. A. Chizhova, P. Geltenbort, A. N. Ivanov, T. Lauer, T. Lins, S. Rotter, H. Saul, U. Schmidt, and H. Abele, Phys. Rev. Lett. **112**, 151105 (2014).
[20] T. Jenke, P. Geltenbort, H. Lemmel, and H. Abele, Nature Phys. **7**, 468 (2011).
[21] M. Kreuz, V. Nesvizhevsky, P. Schmidt-Wellenburg, T. Soldner *et al.*, Nucl. Instrum. Methods Phys. Res. A **611**, 326 (2009).
[22] G. Pignol, S. Baessler, V. V. Nesvizhevsky *et al.*, Adv. High Energy Phys. **2014**, 628125 (2014).
[23] P. Hamilton, M. Jaffe, P. Haslinger, Q. Simmons, H. Müller, and J. Khoury, Science **349**, 849 (2015).
[24] S. Baessler, V. V. Nesvizhevsky, K. V. Protasov, and A. Y. Voronin, Phys. Rev. D **75**, 075006 (2007).
[25] O. Zimmer, Phys. Lett. B **685**, 38 (2010).
[26] A. P. Serebrov, O. Zimmer, P. Geltenbort *et al.*, JETP Lett. **91**, 6 (2010).
[27] S. Afach *et al.*, Phys. Lett. B **745**, 58 (2015).
[28] H. Abele, T. Jenke, H. Leeb, and J. Schmiedmayer, Phys. Rev. D **81**, 065019 (2010).
[29] K. Durstberger-Rennhofer, T. Jenke, and H. Abele, Phys. Rev. D **84**, 036004 (2011).
[30] V. B. Shikin and Yu. P. Monarkha, *Two-Dimensional Charged Systems in Helium* (in Russian) (Nauka, Moscow, 1989).
[31] V. S. Edel'man, Sov. Phys.- Uspehi **130**, 676 (1980).
[32] Y. Monarkha and K. Kono, *Two-Dimensional Coulomb Liquids and Solids* (Springer Verlag, Berlin, 2004).
[33] G. Papageorgiou, P. Glasson, K. Harrabi *et al.*, Appl. Phys. Lett. **86**, 153106 (2005).
[34] B. A. Nikolaenko, Yu. Z. Kovdrya, and S. P. Gladchenko, J. Low Temp. Phys. (Kharkov) **28**, 859 (2002).
[35] A. M. Dyugaev, A. S. Rozhavskii, I. D. Vagner, and P. Wyder, JETP Lett. **67**, 434 (1998).

[36] P. M. Platzman and M. I. Dykman, Science **284**, 1967 (1999); M. I. Dykman, P. M. Platzman, and P. Seddighrad, Phys. Rev. B **67**, 155402 (2003).

[37] L. D. Landau and E. M. Lifshitz, *Course of Theoretical Physics*, Vol. 3, Quantum Mechanics, 3rd ed. (Pergamon Press, Oxford, 1977).

[38] L. D. Landau and E. M. Lifshitz, *Course of Theoretical Physics*, Vol. 6: Hydrodynamics, 2nd ed. (Butterworth-Heinemann, Oxford, 1987).

[39] Yu. P. Monarkha and V. B. Shikin, Low-dimensional electronic systems on a liquid helium surface (Review), Sov. J. Low Temp. Phys. **8**, 279 (1982).

[40] B. E. Clements, H. Godfrin, E. Krotscheck, H. J. Lauter, P. Leiderer, V. Passiouk, and C. J. Tymczak, Phys. Rev. B **53**, 12242 (1996).

[41] E. Eidelstein, D. Goberman, and A. Schiller, Phys. Rev. B **87**, 075319 (2013).

[42] R. Citro, E. Orignac, and T. Giamarchi, Phys. Rev. B **72**, 024434 (2005).

[43] Balazs Dora, Masudul Haque, and Gergely Zarand, Phys. Rev. Lett. **106**, 156406 (2011).

[44] D. A. Ivanov and M. V. Feigel'man, Zh. Eksp. Teor. Fiz. **114**, 640 (1998) [Sov. Phys. JETP **87**, 349 (1998)].

[45] Kazuki Koshino and Tetsuo Ogawa, J. Korean Phys. Society **34**, S21 (1999).

[46] R. Golub, Phys. Lett. A **72**, 387 (1979).

[47] A. M. Dyugaev and P. D. Grigoriev, JETP Lett. **78**, 466 (2003).

[48] A. D. Grigoriev, P. D. Grigoriev, and A. M. Dyugaev, J. Low Temp. Phys. **163**, 131 (2011).

[49] A. D. Grigoriev, P. D. Grigoriev, A. M. Dyugaev, and A. F. Krutov, Low Temp. Phys. **38**, 1005 (2012).

[50] A. F. Andreev, Zh. Eksp. Teor. Fiz. **50**, 1415 (1966) [Sov. Phys. JETP **23**, 939 (1966)].

[51] P. D. Grigoriev, A. M. Dyugaev, and E. V. Lebedeva, Zh. Eksp. Teor. Fiz. **133**, 370 (2008) [Sov. Phys. JETP **106**, 316 (2008)].

[52] P. D. Grigor'ev, A. M. Dyugaev, and E. V. Lebedeva, Pis'ma v Zh. Eksp. Teor. Fiz. **87**, 114 (2008) [Sov. Phys. JETP Lett. **87**, 106 (2008)].

[53] C. C. Chang and M. Cohen, Phys. Rev. B **11**, 1059 (1975); E. Krotscheck, *ibid.* **31**, 4258 (1985); **32**, 5713 (1985); E. Krotscheck and C. J. Tymczak, *ibid.* **45**, 217 (1992); B. E. Clements, E. Krotscheck, and C. J. Tymczak, J. Low Temp. Phys. **107**, 387 (1997).

[54] A. D. Grigoriev, Ph.D. thesis, Samara State University, 2016.

[55] O. Zimmer, F. M. Piegsa, and S. N. Ivanov, Phys. Rev. Lett. **107**, 134801 (2011).

[56] F. M. Piegsa, M. Fertl, S. N. Ivanov, M. Kreuz, K. K. H. Leung, P. Schmidt-Wellenburg, T. Soldner, and O. Zimmer, Phys. Rev. C **90**, 015501 (2014).

[57] K. K. H. Leung, S. Ivanov, F. M. Piegsa, M. Simson, and O. Zimmer, Phys. Rev. C **93**, 025501 (2016).

[58] O. Zimmer, K. Baumann, M. Fertl *et al.*, Phys. Rev. Lett. **99**, 104801 (2007).

[59] O. Zimmer, P. Schmidt-Wellenburg, M. Fertl *et al.*, Eur. Phys. J. C **67**, 589 (2010).

[60] R. Golub and J. M. Pendlebury, Phys. Lett. A **53**, 133 (1975).

[61] R. Golub and J. Pendlebury, Phys. Lett. A **62**, 337 (1977).

[62] M. Daum, P. Fierlinger, B. Franke, P. Geltenbort *et al.*, Phys. Lett. B **704**, 456 (2011).

[63] T. Brenner, S. Chesnevskaya, P. Fierlinger *et al.*, Phys. Lett. B **741**, 316 (2015).

[64] O. Zimmer and R. Golub, Phys. Rev. C **92**, 015501 (2015).

[65] K. P. Hickerson and B. W. Filippone, Nucl. Instrum. Methods Phys. Res. A **721**, 60 (2013).

[66] A. Steyerl, W. Drexel. S. S. Malik, and E. Gutsmiedl, Physica B **151**, 36 (1988).

[67] Y. Arimoto, P. Geltenbort, S. Imajo, Y. Iwashita *et al.*, Phys. Rev. A **86**, 023843 (2012).

[68] C. Siemensen, D. Brose, L. Böhmer, P. Geltenbort, and C. Plonka-Spehr, Nucl. Instrum. Methods Phys. Res. A **778**, 26 (2015).

[69] P. Ch. Bokun, Yad. Fiz. **40**, 287 (1984) [Sov. J. Nucl. Phys. **40**, 180 (1984)].

[70] V. P. Alfimenkov, V. K. Ignatovich, L. P. Mezhov-Deglin, V. I. Morozov, A. V. Strelkov, and M. I. Pulaja, Communications of Joint Institute for Nuclear Research, Dubna preprint P3-2009-197 (2009) [in Russian], available at http://www1.jinr.ru/Preprints/2009/197(P3-2009-197).pdf.

[71] V. F. Ezhov, A. Z. Andreev, G. Ban *et al.*, arXiv:1412.7434.

[72] D. J. Salvat, E. R. Adamek, D. Barlow *et al.*, Phys. Rev. C **89**, 052501 (2014).

[73] K. Leung, S. Ivanov, F. Martin *et al.*, *Proceedings of the Workshop "Next Generation Experiments to Measure the Neutron Lifetime", Santa Fe, New Mexico, 9–10 November 2012* (World Scientific, Singapore, 2014), p. 145.

[74] V. F. Ezhov, A. Z. Andreev, G. Ban *et al.*, Nucl. Instrum. Methods Phys. Res. A **611**, 167 (2009).

[75] K. K. H. Leung and O. Zimmer, Nucl. Instrum. Methods Phys. Res. A **611**, 181 (2009).

[76] R. Picker, I. Altarev, J. Bröcker *et al.*, J. Res. NIST **110**, 357 (2005).

[77] P. R. Huffman, C. R. Brome, J. S. Butterworth *et al.*, Nature **403**, 62 (2000).

[78] O. Zimmer, J. Phys. G: Nucl. Part. Phys. **26**, 67 (2000).

[79] F. E. Wietfeldt and G. L. Greene, Rev. Mod. Phys. **83**, 1173 (2011).

[80] S. Paul, Nucl. Instrum. Methods Phys. Res. A **611**, 157 (2009).